Photoinduced Processes in Hydrogen Bonded System: Photodissociation of Imidazole Clusters†

Viktoriya Poterya, Václav Profant, and Michal Fárník*

J. Heyrovský Institute of Physical Chemistry, v.v.i., Academy of Sciences of the Czech Republic, Dolejškova 3, 182 23 Prague 8, Czech Republic

Lukáš Šištík and Petr Slavíček‡

Department of Physical Chemistry, Institute of Chemical Technology Prague, Technická 5, Prague 6

Udo Buck

Max-Planck Institut für Dynamik und Selbstorganisation, Bunsenstrasse 10, D-37073 Göttingen, Germany

Received: May 4, 2009; Revised Manuscript Received: June 10, 2009

The photodissociation of imidazole in hydrogen bonded clusters has been studied at photodissociation wavelengths 243 and 193 nm. Imidazole clusters of different mean cluster sizes $\bar{n} \approx 3$ and 6 have been produced in expansions with He and Ar carrier gases, and the mean cluster sizes were determined by mass spectrometric and crossed beam scattering experiments. Simultaneously, the $(C_3N_2H_4)_n$ clusters were studied by ab initio calculations for n up to 4 molecules, confirming the hydrogen bond N−H···N motif in the clusters. The measured H-fragment kinetic energy distribution spectra exhibit a bimodal character similar to the KEDs found for the bare molecule.[1] At 243 nm the fast H-atoms originate from the direct dissociation process on the repulsive $\pi\sigma^*$ state, and the slow component results from the dynamics populating the vibrationally hot ground state via an S_1/S_0 conical intersection. In the clusters the contribution of the slow component increases with the cluster size. The slow component is also dominant at the shorter wavelength of 193 nm, where the dynamics starts with the excitation of $\pi\pi^*$ state. It is shown that the slow component in our experiment is a product of subsequent two-photon absorption. We have proposed different mechanisms how the observed enhanced internal conversion can be rationalized. The increased stability with respect to the H-fragmet dissociation in clusters can be caused either by hydrogen transfer in the N−H···N bond or by closing the $\pi\sigma^*$ dissociation channel as in the case of pyrrole clusters.

I. Introduction

Five-membered, nitrogen containing rings, such as pyrrole, pyrazole, or imidazole represent important chromophoric groups. The reason is their significance in biological processes. The structural motif of the imidazole (Im) molecule $C_3N_2H_4$ can be found in many biological compounds: it forms a side chain of histidine, it is part of histamine or purine (and consequently of adenine and guanine). Imidazole is, for example, also an important ligand toward transition metal ions in vitamin B_{12} and we find the imidazole unit also in urocyanic acid, the natural sunscreen absorbing UV light in the skin.

It is therefore not surprising that the photoinduced processes in this molecule has been frequently studied both experimentally[1−4] and theoretically.[5−8] Imidazole UV dissociation dynamics in the gas phase has been studied by Devine et al.[1] in the wavelength range 240−210 nm and at 193 nm by high resolution photofragment spectroscopy. The role of the excited $\pi\sigma^*$ states in the photodissociation of imidazole and similar molecules (pyrrole and phenol) has been discussed by the same group.[2] The general picture of imidazole photochemistry emerges as follows (see schematic picture of photodissociation processes possible upon excitation with wavelengths relevant for the present experiment, Figure 1). Upon the threshold photoabsorption, the imidazole photodynamics is dominated by the $\pi\sigma^*$ state (around 240 nm). This state is dissociative, and

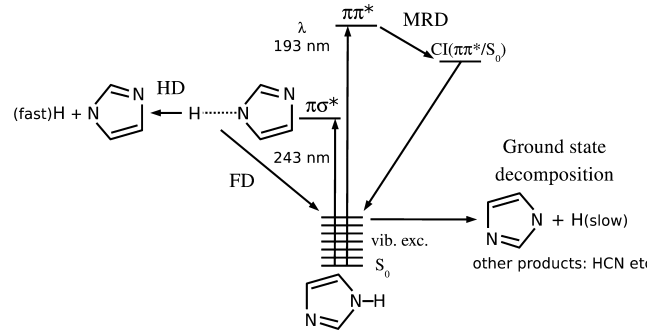

Figure 1. Schematic picture of photodissociation processes possible in the imidazole molecule upon excitation with wavelengths relevant for the present experiment. At 243 nm the $\pi\sigma^*$ state is excited, leading to the direct hydrogen dissociation (HD) and fast H-atom production. Alternatively, frustrated dissociation (FD) can occur via a $\pi\sigma^*/S_0$ conical intersection at alongated N−H distances. At higher photon energies, the $\pi\pi^*$ state is populated and molecular ring distortion (MRD) can occur, quenching the molecule into the vibrationally hot ground state.

† Part of the "Vincenzo Aquilanti Festschrift".

* Corresponding author. E-mail:michal.farnik@jh-inst.cas.cz.

‡ E-mail: petr.slavicek@vscht.cz. Also affiliated at J. Heyrovský Institute of Physical Chemistry, v.v.i., Academy of Sciences of the Czech Republic, Dolejškova 3, 182 23 Prague 8, Czech Republic.

10.1021/jp904145q
Published on Web 07/02/2009

Figure 2. Hydrogen bonding motifs in pyrrole and imidazole clusters.

as a result, the hydrogen atom is released (hydrogen dissociation, HD, channel). At alongated N−H distances, the $\pi\sigma^*/S_0$ intersection occurs. It is therefore possible that frustrated dissociation (FD) takes place, and the molecular ground state is recreated. At higher photon energies, the $\pi\pi^*$ state (centered around 206 nm) is populated. A molecular ring distortion (MRD) reaction channel is opened. Subsequently, the molecule quenches into the vibrationally hot ground state, where again the H-atom can dissociate or the molecule can decompose to other fragments.

The role of $\pi\sigma^*$ states in gas phase biomolecules has attracted significant attention and its role in biophysics was discussed.[9] The functionality of biomolecules is, however, controlled by its environment, either by a solvent or by specific interactions with other molecular units (such as hydrogen bonding in DNA base pairs). Photochemistry in solvated systems can be quite different. For example, we have recently demonstrated in a joint experimental and theoretical study of pyrrole clusters[10] that the $\pi\sigma^*$ state of a Rydberg character is closed upon solvation with other pyrrole molecules or argon atoms. A very similar effect has been also observed at the same time in the group of Kitsopoulos[11,12] by solvating the pyrrole molecule with a single Xe atom.

The type of interaction found in pyrrole clusters (N−H···π interaction) or pyrrole−rare gas clusters represents the simplest type of solvation, in which the chromophore does not react with the solvent. If, however, the N−H bond is involved in hydrogen bonding, the hydrogen atom of the donor molecule can migrate to the acceptor molecule and new phenomena can occur. This is the case for pyrrole···ammonia,[13] pyrrole···water,[14] or pyrrole···pyridine complexes.[15] Here, we study imidazole clusters in which the N−H···N hydrogen bond defines the structure. Figure 2 illustrates the different bonding motifs in pyrrole and imidazole clusters.

The major focus of the present paper is to investigate the photodissociation of imidazole in clusters while varying the mean cluster size. First, we determine the mean cluster sizes in mass spectrometric and crossed beam scattering experiments. Then the H-fragment kinetic energy distributions are measured after the imidazole cluster photodissociation. The clusters are also studied theoretically. Their structures are calculated and the measured spectra analyzed using a simple statistical model. The joint experimental and theoretical treatment yields a detailed insight into the photodissociation dynamics of imidazole in clusters.

The paper is organized as follows: In the next section we introduce the applied experimental and theoretical methods. Then we discuss the calculated cluster structures. When discussing the experimental results, we first determine the mean cluster sizes corresponding to the various expansion conditions, and then the results of the photodissociation experiment are presented and discussed. Finally, conclusions are drawn.

II. Methods

A. Experiment. The experimental apparatus was built and used previously in the Max-Planck Institute in Göttingen[16−19] and moved to the J. Heyrovský Institute in Prague.

The clusters are produced by a supersonic expansion through a conical nozzle 55 μm in diameter, 2 mm long, and 30° opening angle. Imidazole is solid at room temperature and atmospheric pressure. Therefore, a new beam source has been designed and built for producing clusters of molecules from solid samples with sufficiently high vapor pressures at moderate temperatures, namely, clusters of small biomolecules. It consists of a reservoir oven heated to a constant temperature T_R inside the vacuum chamber. The carrier gas passes through the reservoir containing the sample and the vapor mixture is carried to the nozzle through a 90 mm long tube with 3 mm inner diameter. The tube and the nozzle are heated separately from the reservoir to a constant temperature T_0. The nozzle temperature is slightly higher (typically by 20 K) than the reservoir temperature to prevent condensation in the nozzle. In the present experiments Ar or He was used as carrier gases, and T_R and T_0 were varied in the range 375−435 and 400−455 K, respectively, to produce different cluster size distributions. Selected expansion conditions are summarized in Table 1 and discussed in section IIIB.

After passing through a skimmer followed by two differentially pumped vacuum chambers, the cluster beam enters a transversely mounted Wiley−McLaren time-of-flight spectrometer (WMTOF). In the extraction region of the WMTOF the clusters interact with the UV photons, are photodissociated and the H-fragments are ionized and detected. The WMTOF spectrometer is operated in the low-field mode with a small electric field 7.9 V cm^{-1} to measure the time-of-flight (TOF) spectra of the H-fragments. The spectrometer can be also operated in the high-field mode ($\approx$200 V cm^{-1}) as a TOF mass spectrometer to detect the ionized fragments after multiphoton cluster ionization. Alternatively, the clusters can be electron impact ionized in the following vacuum chamber and the mass spectra of the ionized cluster fragments can be recorded by a quadrupole mass spectrometer.

The photodissociation experiment is performed with the primary cluster beam without the scattering size selection; however, the mean cluster sizes are known from the scattering experiment described below. The imidazole molecules in clusters are photodissociated, and the arising H-fragments are efficiently ionized at the same wavelength of 243.07 nm (one-color resonance enhanced multiphoton ionization, REMPI, in the 2 + 1 excitation scheme). The laser pulses of this wavelength are generated by mixing the fundamental 1064 nm of a Nd:YAG laser with the frequency doubled output of a dye laser pumped by the second harmonics of the Nd:YAG laser, and operated at 630 nm. The system produces laser pulses of 5 ns duration at 10 Hz repetition rate. The typical energy employed in the present experiments was 0.7 mJ/pulse in the interaction region. The laser beam is focused into the vacuum chamber with a 400 mm quartz lens onto a 14 μm spot (Gaussian beam waist). The tight focus results in high photon fluxes of approximately 10^{28} s^{-1} cm^{-2}.

Alternatively, the imidazole is dissociated at 193.3 nm, generated by an ArF/F_2-Excimer laser, and the H-fragments are subsequently ionized by the 243 nm laser pulse. The 193 nm laser beam is focused by a 366 mm LiF lens to a spot of about 10^{-4} cm^2 at the intersection with the molecular beam and the 243 nm beam. The maximum energy of the 193 nm radiation

TABLE 1: Experimental Conditions for Producing Imidazole Clusters and Their Corresponding Mean Sizes

nozzle diameter, d 55 = μm			length, l = 2 mm		opening angle, α = 30°
carrier gas	pressure, p_0 (bar)	nozzle temp, T_0 (K)	reservoir temp, T_R (K)	imidazole conc, c (%)	mean cluster size, $\bar{n}$
He	2.6	435	420	1.7	≤2
He	2.6	435	435	4.1	3
Ar	2.0	455	435	5.4	6

at the interaction region was about 10 mJ over the 25 ns long laser pulse, corresponding to a photon flux of about 10^{27} s^{-1} cm^{-2}.

The laser pulses are synchronized using a pulse delay generator so that the 193 nm pulses preceded the 243 nm ones by 5−20 ns. The spatial and time overlap of the two laser beams and the molecular beam are adjusted on the maximum signal and a symmetric shape of the H-fragment spectrum from the well studied $(HBr)_n$ test system.[20]

In the data analysis process the measured TOF spectrum is converted to the kinetic energy distribution (KED) of the fragment H-atoms. The analysis involves a complete Monte Carlo (MC) simulation of the particle trajectories, which is carried out, considering the molecular beam data, the photodissociation process parameters, the WMTOF geometry, the finite interaction volume, and the detector electronic response.[20]

To determine the mean cluster sizes at various expansion conditions, a scattering experiment in a crossed-beam arrangement was performed. The method, originally introduced by Buck and Meyer,[21] was employed to determine the mean sizes of various rare gas and molecular clusters; e.g., recently, pyrrole clusters were studied in our lab.[22] Briefly, the skimmed cluster beam was crossed perpendicularly by a beam of He atoms. In elastic collisions the clusters of different sizes were scattered into different laboratory (LAB) angles: in principle, the smaller, i.e., lighter, clusters were scattered into the larger angles. The clusters scattered at a particular LAB angle were allowed to proceed to the following vacuum chambers for detection by means of the quadrupole mass-spectrometer. Choosing an appropriate scattering angle could exclude clusters *larger* than a certain corresponding size from the detection. In addition, clusters *smaller* than a certain size could be excluded from the detection by selecting an appropriate fragment mass. Thus only clusters from a defined cluster size range were detected. By an analysis of the measured mass spectra and LAB angular distributions for various ionic cluster fragments, the mean cluster sizes could be obtained.[23]

B. Calculations. The dominant interaction between imidazole molecules is hydrogen bonding. This structural motif can lead to a specific photochemical behavior. We have therefore performed ab initio calculations of small imidazole clusters (with one to four imidazole units). Essentially two questions were addressed: (i) what is the energetics of the hydrogen bonding in imidazole clusters, and (ii) what are the geometrical features of the larger imidazole clusters?

For the imidazole dimer, the interaction energies were calculated at the CCSD(T) and MP2 level with different basis sets. We then tested the performance of various density functional approaches, including the new M06 family of functionals,[26] double hybrid functionals,[27] and dispersion corrected functionals.[27] The binding energies of larger imidazole clusters were then calculated with B3LYP-D method, in which the dispersion contribution of interaction energy is added at the empirical level.[27,28]

Ab initio calculations were also used to model the hydrogen dissociation from the ground state. The slow component of the measured kinetic energy distribution spectra were compared with KED spectra calculated under the assumption that the dissociation was a statistical process taking place from the ground state. A similar approach was adopted that was used to model a statistical decay of a single imidazole molecule in the vibrationally hot ground state in the work by Devine et al.[1] We considered dissociation at energies E corresponding to one or two photons, i.e., 5.1, 6.4, 10.2, and 12.8 eV. The calculation was done in a rather crude way: the probability of finding hydrogen with a kinetic energy ε_k at energy E was calculated as

$$P(\epsilon_k,E) \propto \Omega(E - \epsilon_k) \cdot \sqrt{\epsilon_k} \quad (1)$$

i.e., the probability was proportional to the density of states of the hydrogen atom with a given kinetic energy and the density of the states of the rest of the molecule that carries the energy $E - \varepsilon_k$. Several rather serious approximations were involved in this treatment.[29−31] First, the conservation of angular momentum was not taken into account.[29] Second, the density of states of the fragment radical was modeled within the harmonic approximation, which was not fully adequate at such high energies. Third, we considered that the species formed upon the dissociation were the imidazoyl radical and hydrogen atom. This was very likely not the case; the imidazole structure could open and the molecule could even fragment, e.g., HCN and C_2NH_3 can be easily formed. Further simplifications used in such calculations are discussed in more detail e.g., in refs 29−31. Nevertheless, the calculations turned out to be in reasonably good agreement with the experimental spectra and they were also robust with respect to the fragment choice. Actually, in such statistical oscillator processes it was commonly just the total number of modes that mattered as far as the oscillator density of states was concerned. These calculations could thus provide a first-order approximation picture about the energetics of the processes in the clusters (see the discussion of photodissociation in section IIIC).

Ab initio calculations were performed using following packages: Gaussian03,[32] ORCA[33] (double hybrid functionals and dispersion corrected functional), and NWCHEM[34] (M06 functionals).

III. Results and Discussion

A. Structural Features of Imidazole Clusters. For the imidazole dimer, MP2 and CCSD(T) interaction energies were compared with various density functionals. The binding energies are summarized in Table 2. Basis set superposition errors were always included. Since the intermolecular bonding is dominated by the electrostatic interaction between imidazole units, it is not surprising that the interaction energy is reasonably converged already for a small basis. As a benchmark for subsequent DFT calculations, we took the MP2/aug-cc-pVTZ level, yielding the interaction energy of 10.0 kcal/mol. This value is close to that obtained by double hybrid functionals B2PLYP and mPW2PLYP and even better agreement is obtained with the density functional methods complemented with an empirical dispersion correction

TABLE 2: Interaction Energy of Imidazol Dimer Evaluated at the MP2/aug-cc-p VDZ Geometry with Different DFT Approaches and with Different Bases

	E_{int}, kcal mol^{-1}		
	6-31+G*	aug-cc-p VDZ	aug-cc-p VTZ
MP2	−9.05	−9.64	−10.00
CCSD(T)	−7.81	−8.84	
B3LYP	−8.05	−7.99	−7.91
BMK	−7.90	−7.61	−7.72
BhandHLYP	−8.45	−8.32	−8.45
B2PLYP	−8.57	−8.73	−8.95
mPW2PLYP	−9.11	−9.18	−9.37
B3LYP-D	−9.92	−9.94	−9.72
PBE-D	−10.12	−10.33	−10.19
M06-HF	−9.25	−8.75	−8.49
M06−2X	−8.77	−8.40	−8.56

(B3LYP-D, PBE-D). The structure and energetics of all larger clusters was therefore optimized on the B3LYP-D level.

Figure 3 shows calculated geometries of selected imidazole clusters together with the corresponding binding energies. It is instructive to compare the structure of imidazole clusters with the structure of isoeletronic pyrrole clusters (see also Figure 2). While for pyrrole clusters, the major structural motif is the N−H bond pointing toward the π system of the second pyrrole unit, for imidazole we observe a true hydrogen bond. The imidazole planes are perpendicularly oriented for the dimer (see also ref 35). Larger clusters can be formed in either linear or cyclic arrangements. In the linear chains, two subsequent imidazole units are again perpendicularly oriented, while the angle between the respective planes is smaller for the cyclic structures. For all the studied clusters, the cyclic structures were lying lower in energy than the linear structures. Energetically, the imidazole clusters show stronger binding energies than pyrrole clusters by a factor of 2−3. The different structural motifs might be expected to change significantly the photochemical behavior of the imidazole clusters.

B. Mass Spectrometry and Cluster Size Distributions. The focus of the present study was to investigate the effect of the cluster environment on imidazole photodissociation and its

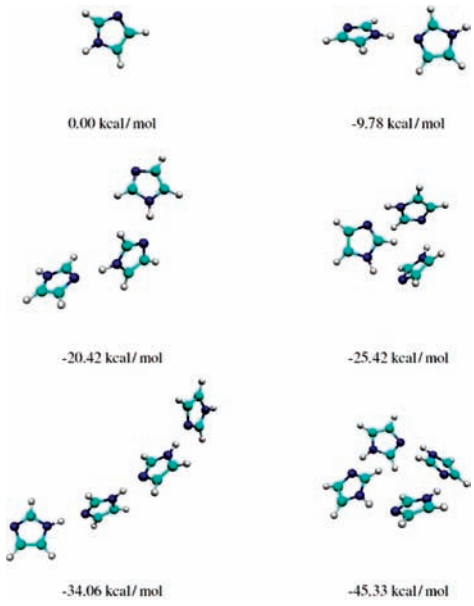

Figure 3. Calculated geometries of selected imidazole clusters at B3LYP-D/aug-cc-pVDZ level of theory. The BSSE corrected binding energies are shown in kcal/mol.

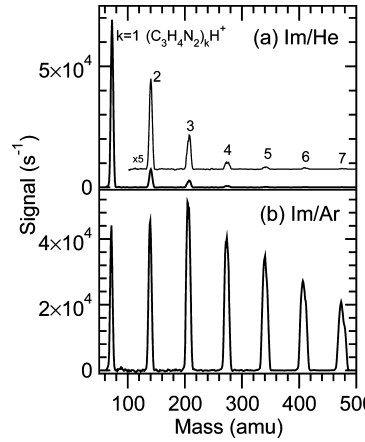

Figure 4. Mass spectra of imidazole clusters generated in supersonic expansions of $C_3H_4N_2$ (a) in helium at 2.6 bar He pressure, imidazole reservoir temperature T_R = 435 K (4.1% $C_3H_4N_2$ in He) and nozzle temperature T_0 = 455 K, and (b) in argon at 2.0 bar Ar pressure, T_R = 435 K (5.4% $C_3H_4N_2$ in Ar), T_0 = 455 K.

dependence on the cluster size. Therefore, imidazole clusters of different sizes were produced under various expansion conditions. In this section we determine the generated mean cluster sizes. In particular, we used expansions in helium and argon carrier gases to produce smaller and larger clusters, respectively. Selected expansion conditions and the corresponding mean cluster sizes are summarized in Table 1.

The electron impact ionization of the cluster beam and subsequent quadrupole mass spectrometry together with the scattering experiment were utilized to yield insight into the cluster size distribution and composition. Figure 4 shows the mass spectrum of imidazole clusters generated in supersonic expansions of imidazole in helium at 2.6 bar He pressure, reservoir temperature T_R = 435 K and nozzle temperature T_0 = 455 K. These conditions correspond to 4.1% $C_3H_4N_2$/He mixture expansion. It should be noted that the quadrupole resolution was degraded in these spectra to obtain a constant high transmission over the entire mass region. Carefully calibrated mass spectra with higher resolution indicated that protonated fragments $(C_3H_4N_2)_kH^+$ dominate the spectra, which is also confirmed by our high resolution TOF mass spectra after multiphoton ionization discussed below. Angular distributions after scattering with a He-atom beam have been meassured for $(C_3H_4N_2)_kH^+$, k = 1−3 fragments. The analysis of the mass spectra and angular distributions and their comparison with our previous measurement of pyrrole clusters[22] yield an average cluster size of $\bar{n} \approx 3$.[36] The distribution has an exponential character which means that there are still more than twice as much monomers than trimers but also larger sizes up to at least n = 6 in the beam.

For comparison, we wanted to investigate the photodissociation of only the bare molecules in our experiment. Therefore, we have lowered the reservoir temperature to expand less concentrated imidazole mixtures in He. This, however, lowers dramatically the photodissociation signals.[37] Reasonably good photodissociation signals could still be observed at T_R = 419 K, which corresponds to the imidazole concentration of 1.7%, but the mass spectrum measured under these conditions does not differ significantly from the spectra in Figure 4a. The same holds for the measured angular distributions. Thus the clusters probably still contribute to the spectra measured under these conditions, yet the photodissociation spectra discussed below

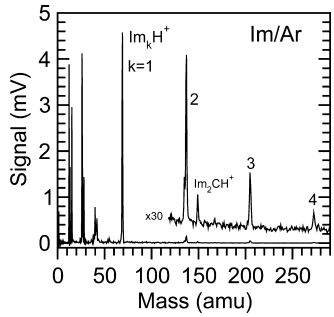

Figure 5. Multiphoton ionization mass spectrum measured at 193 nm with the WMTOF mass spectrometer. The imidazole clusters were generated in supersonic expansions of $C_3H_4N_2$ in argon at 2.0 bar Ar pressure, $T_R = 435$ K, and $T_0 = 455$ K.

indicate that somewhat smaller species were probed. Therefore, we tentatively assign the mean cluster size for these conditions to $\bar{n} \leq 2$.

Figure 4b shows the mass spectrum of imidazole clusters generated in argon expansions at 2.0 bar, reservoir temperature $T_R = 435$ K, and nozzle temperature $T_0 = 455$ K. These conditions correspond to the 5.4% $C_3H_4N_2$/Ar mixture. Here the larger clusters are produced, for which the analysis of the angular distributions measured in the scattering experiment is complicated by the limited angular distribution. However, we notice that the $(C_3H_4N_2)_kH^+$ fragments occur at the threshold angles for $(C_3H_4N_2)_n$ neutral clusters with $n = k + 2$; i.e., fragments of size k originate from the neutral clusters of sizes larger by at least two molecules, i.e., $n \geq k + 2$. Therefore, we evaluate the neutral cluster mean size $\bar{n}$ from the mean size of the ionized fragments from the mass spectrum $\bar{k} \approx 4$ as $\bar{n} \approx k + 2 = 6$. We note that this is rather a lower boundary for the neutral cluster mean size generated in the Ar expansion. It is also worth mentioning that the measured angular distributions suggest that the protonated monomer fragments $(C_3H_4N_2)H^+$ originate apparently only from larger clusters $n \geq 6$.

The presence of the larger clusters in the beam could also be verified by multiphoton ionization at 193 nm utilizing our WMTOF spectrometer in the high field mode as the mass spectrometer. The corresponding mass spectrum of imidazole clusters generated in Ar expansions under the above conditions is shown in Figure 5. The resolution of our TOF mass spectra allows us to determine unambiguously the observed fragments as the protonated species $(C_3H_4N_2)_kH^+$. The ionization potential of imidazole is 8.8 eV.[3] Therefore, an absorption of at least two 193 nm photons (2 × 6.4 eV) is required to ionize the clusters, which is quite in agreement with the photodissociation experiment discussed below, where successive two-photon processes have to be implicated to explain the measured KEDs.

We have noted that the ionization by two or more successively absorbed photons usually leads to a higher degree of fragmentation of the ionized species than the electron impact ionization (even with 70 eV electron energy). We have observed this behavior consistently for pyrrole,[22] imidazole, pyrazole, and phenol molecules and clusters. The more surprising is the fact that we could observe protonated imidazole clusters as cluster fragments in our multiphoton ionization TOF mass spectra, despite the more extensive fragmentation. This was not the case for pyrrole clusters, where masses above the monomer ion were not observed in the TOF mass spectra even for larger clusters. This in turn points to probably larger and definitely more strongly bound cluster species generated from imidazole molecules than from pyrrole. Also Devine at al.[1] discuss photoionization-TOF mass spectrometry. However, they have observed

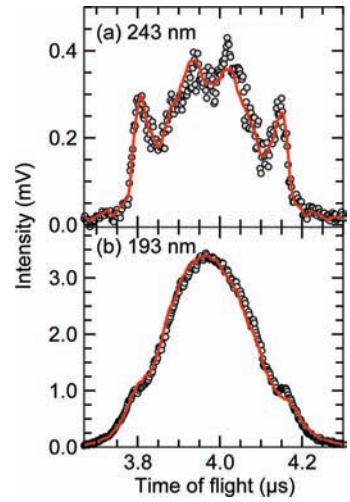

Figure 6. Example of the measured H-fragment TOF spectrum measured at (a) 243 nm and (b) 193 nm. The imidazole clusters were generated in He expansions at $p_0 = 2.6$ bar, $T_R = 435$ K (4.1% $C_3H_4N_2$ in He), and $T_0 = 455$ K.

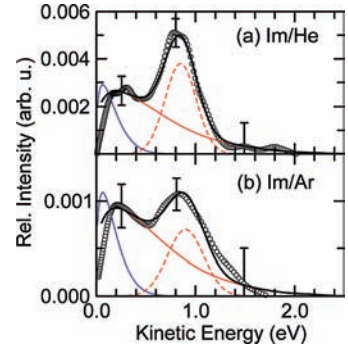

Figure 7. H-fragment KED from photodissociation of imidazole clusters at 243 nm: (a) clusters generated in He expansion corresponding to the mean cluster size $\bar{n} = 3$, (b) clusters generated in Ar expansion, mean cluster size $\bar{n} = 6$. The solid blue and red lines correspond to the statistical model calculations assuming an excitation energy of 5.1 and 10.2 eV, respectively; the dashed red line corresponds to a Gaussian fit of the fast component and the solid black line shows the sum of the red components fitting the experiment.

no detectable ion signal at 193 nm, which might be due to their lower laser pulse energies and subsequently single-photon processes only.

C. Cluster Photodissociation. In the photodissociation experiment we have studied the dependence of the process on the photodissociation wavelength (243 and 193 nm) and on the cluster size. Figure 6 shows an example of the measured H-fragment TOF spectrum of imidazole clusters generated in He expansions corresponding to the mean cluster size $\bar{n} \approx 3$ photodissociated at 243 nm (a) and 193 nm (b). The measured points were fitted with the MC-simulation (red line) mentioned in the section 2.1 to obtain the H-atom KED shown in Figures 7a and 8a. The TOF spectrum illustrates the signal-to-noise ratio in the raw data, which is then represented by error bars on selected points in the converted KEDs. It can be immediately seen in the spectrum of Figure 7a that it has a bimodal character with the outer peaks at approximately 3.81 and 4.15 μs, which correspond to the faster H-fragments, and the inner peaks around 4 μs corresponding to the slow fragments. On the energy scale these fast and slow fragments peak at about 0.85 and 0.25 eV, respectively.[38] Similar spectra were measured at the other expansion conditions.

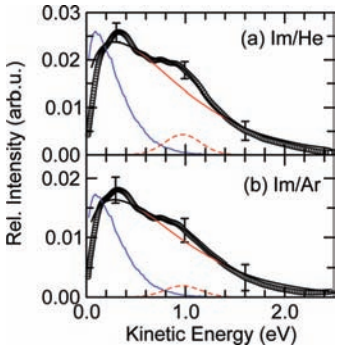

Figure 8. H-fragment KED from photodissociation of imidazole clusters at 193 nm: (a) clusters generated in He expansion corresponding to the mean cluster size $\bar{n} = 3$; (b) clusters generated in Ar expansion, mean cluster size $\bar{n} = 6$. The solid blue and red lines correspond to the statistical model calculations assuming an excitation energy of 6.4 and 12.8 eV, respectively; the dashed red line corresponds to a Gaussian fit of the fast component and the solid black line shows the sum of the red components fitting the experiment.

Figure 7 shows the H-fragment KED from photodissociation of imidazole clusters at 243 nm for two different mean cluster sizes: (a) $\bar{n} \approx 3$, clusters generated in He expansion, and (b) $\bar{n} \approx 6$, clusters generated in Ar expansion. The H-fragment KED from photodissociation of imidazole clusters at 193 nm is shown in Figure 8. Again the top spectrum (a) originates from the clusters generated in He expansion corresponding to the mean cluster size $\bar{n} \approx 3$, and the bottom one (b) to the clusters generated in Ar expansion, $\bar{n} \approx 6$.

The KEDs in Figures 7 and 8 were analyzed in terms of contributions of the slow (solid red lines) and fast (dashed red lines) fragments. The previous photodissociation study of the imidazole molecule at similar wavelengths by Devine et al.[1] has shown that the fast fragments originate from a direct N−H bond fission process, while the slow component was attributed to the statistical decay of highly vibrationally excited ground state molecules. In our spectra the fast component corresponding to the direct process was fitted with a Gaussian peak and the slow component was calculated assuming a statistical decay model outlined in section IIB.

The agreement of the statistical decay model with the measured slow component KED both for the single imidazole molecule[1] and for the present clusters strongly suggests the conversion to the hot ground state. However, an excited state dynamics, which would yield the slow fragments cannot be entirely ruled out on the basis of this experimental evidence. Nevertheless, we cannot see an indication for such an excited state dissociation channel leading to the slow fragments on the available PES, and therefore it would have to proceed along some other than the N−H coordinate. It is also worth noting that such slow-component KED are quite typical for fragments departing from species with high energy content, e.g., for thermal electrons emitted from energy-rich clusters.[30,31]

The blue lines show the calculated KEDs assuming the energy corresponding a single photon excitation, i.e., 5.1 and 6.4 eV for the 243 and 193 nm, respectively. Apparently, the statistical decay assuming just a single photon excitation would yield much slower H-fragments, than observed experimentally. A better agreement with the experiment could be obtained, assuming a higher excitation energy. The red curves correspond to the calculations with twice the photon energy, i.e., assuming a two-photon excitation. The agreement with the experiment is within the indicated experimental errors.

Several factors can account for the remaining small discrepancies: (i) The lower energy maximum at about 0.25 eV is somewhat sharper in the experimental KEDs especially for the 193 nm data. Taking twice the photon energy in the calculations assumes no energy dissipation before the absorption of the second photon. More likely, some of the energy is dissipated in the cluster before the second photon absorption. This process has been been observed recently in our laboratory for acetylene clusters.[39] Thus the total energy from which the statistical decay proceeds can be lower. Note the sharper distribution for single photon excitation, i.e., 6.4 eV. Our calculations show sharper distributions similar to the experimental one for energies around 8 eV; however, the position of the maximum is also shifted to somewhat lower values. Besides, photons of 243 nm may be also present in the interaction region in the experiment with 193 nm and thus the total energy might correspond to the combination of these two energies. Therefore, the slow component in the experiment is very likely a convolution of statistical processes with different energies between 6.4 and 12.8 eV. (ii) In addition, it is also probable that both one- and two-photon processes occur simultaneously, which would lead to a sharper distribution; however, again, the maximum would be also shifted to lower values, (iii) Finally, the statistical model is only approximate as discussed in the calculation section.

Nevertheless, it can be concluded that assuming a statistical decay model for molecules excited at energies corresponding to approximately twice the photon energy, the slow component in the experimental data could be fitted very well. Thus the subsequent two-photon processes play a major role in the generation of the slow H-fragments in our experiment.

Here we justify the assumption of the successive multiphoton processes in our experiment. At the present 243 nm photon flux of 10^{28} s^{-1} cm^{-2} and pulse duration of 5 ns the absorption cross section of an imidazole molecule (cluster) would have to be $\sigma \approx 4 \times 10^{-20}$ cm^2 so that two photons could be absorbed successively by the molecule (cluster) within a single laser pulse. In addition, from the relative cross section in Figure 1 in ref 1 it follows that the cross section at 193 nm is more than 10 times larger than at 243 nm. Therefore, if the two-photon processes at 243 nm are observed, the multiphoton processes at 193 nm will be observed too.

The successive multiphoton hydrogen generation is only possible if the dynamics proceeds on the ground state PES, where the excited species survive long enough to ensure the absorption of the second photon. Therefore, the multiphoton character is inherent to the slow component of the measured KEDs. On the other hand, if the dissociation proceeds quickly on the repulsive PES of the excited $\pi\sigma^*$ state, the H-fragment departs before the second photon can be absorbed by the cluster.

It is worth noting that in the case of the single photon processes yielding the slow component it would be more clearly separated from the fast one, as observed by Devine et al.[1] for the imidazole molecule. Their UV pulse energies 0.2−2.5 mJ were somewhat lower than in the present experiment, which probably led to exclusively single photon processes. However, it is not the pulse energy but rather the photon flux density, which should be compared, yet this parameter is not available in ref 1. We note that our theoretical calculations of KED assuming the statistical decay after a single photon processes (blue curves in Figures 7 and 8) yield clearly separated slow and fast component quite in agreement with the spectra in ref 1.

On the other hand, several arguments can be mentioned for why more then two-photon processes are not considered. The KED simulations with energies corresponding to absorption of three photons yield fragments with too much energy exceeding the measured spectra. The processes with more than two photons

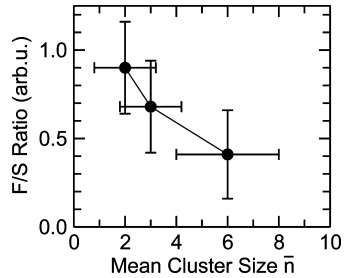

Figure 9. Fast-to-slow peak ratio obtained by integration of the measured KEDs.

can probably lead to efficient ionization. This may be partially true even for the two-photon processes. The ionization will compete with the photodissociation process (see, e.g., the photoionization mass spectrum in Figure 5 and its discussion) and probably prevails at the higher energies, i.e., with the larger number of photons absorbed. Besides the higher number of absorbed photons may lead to a total destruction of the molecule to fragments other than the H-atom and the imidazolyl radical. Therefore, mostly successive two-photon absorption processes correspond to the slow component in the KEDs.

Separating the KEDs into the contributions from slow and fast fragments, the relative ratio of these contributions in dependence on the mean cluster size and on the photodissociation wavelength can be discussed. From Figure 7 it is apparent that the contribution of the fast processes decreases with the increasing cluster mean size. Quantitatively, this ratio F/S was evaluated by integrating the fitted spectra components and plotted in Figure 9 as a function of the mean cluster size. In this plot also the ratio is shown from another spectrum measured at the lower reservoir temperature $T_R = 435$ K. As discussed above, these conditions correspond to $\bar{n} \leq 2$, and this point is plotted in the F/S graph at $\bar{n} = 2$. At 193 nm the slow fragments strongly dominate the spectra in Figure 8. The fast component is still discernible in the KEDs and could be fitted; however, the F/S ratio is very small, and therefore it is difficult to asses quantitatively its dependence on the cluster size.

As discussed above, the fast component originates from direct dissociation of hydrogen atom in the excited state. The slow component is a result of a two-step process, in which the molecule first quenches into the vibrationally hot ground state and here it dissociates. Apparently, the direct dissociation is suppressed and/or quenching into the ground state enhanced in clusters. There are two basic mechanisms for how this can happen: enhanced frustrated dissociation (EFD) and newly opened hydrogen transfer (HT) mechanism; see Figure 10. In the EFD mechanism, the hydrogen atoms leaving the excited molecule can be mechanically prevented from the dissociation by surrounding molecules. Instead of dissociating, the imidazole ground state can be reconstructed via the $\pi\sigma^*/S_0$ intersection. This mechanism is also possible in the isolated molecule (see Figure 1); however, it can be substantially enhanced upon complexation in the H-bonded cluster. The $\pi\sigma^*/S_0$ conical intersection is furthermore expected to be shifted up in energy. The dissociative reaction path will be therefore less important in clusters than for isolated imidazole. The ground state can also be formed via $\pi\pi^*/S_0$ intersection occurring upon molecular ring distortion (MRD). This reaction path is not affected by the complexation. The mechanisms outlined above explain the disappearance of the direct dissociation for pyrrole clusters.

There is, however, another possible mechanism for hydrogen bonded systems. In the hydrogen transfer (HT) mechanism, the dissociating hydrogen atom is transferred to the second imidazole molecule along the hydrogen bond reaction coordinate. At this point, the S_1/S_0 conical intersection is reached, imidazole in the ground state is formed, and ultrafast hydrogen transfer back to the original molecule occurs. Our preliminary calculations suggest that this second mechanism is open upon the excitation into the (bright) $\pi\pi^*$ state and ultrafast hydrogen transfer can occur. If the molecule is excited into the (dark) $\pi\sigma^*$ state, the hydrogen transfer is still a barrierless process; however, the driving force for HT is negligible. Upon this excitation into the $\pi\sigma^*$ state the hydrogen bond pattern immediately destructs and the H-transfer cannot proceed.

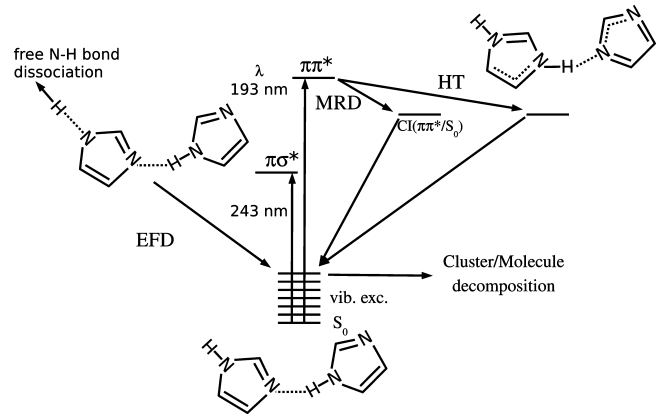

Figure 10. Schematic picture of photodissociation processes possible in imidazole clusters (dimer). At 243 nm, the $\pi\sigma^*$ state of an imidazole molecule is excited, leading to the direct free hydrogen dissociation. However, the frustrated dissociation may be enhanced by the cluster environment (EFD). At higher photon energies, the $\pi\pi^*$ molecular state is populated. In addition to the molecular ring distortion (MRD) channel present for the molecule, also the hydrogen transfer (HT) channel can occur in the cluster.

Imidazole thus represents an interesting example in which the photochemical pathways are controlled by the excitation wavelength for the isolated molecule, where the S_1 photochemistry is different from the $\pi\pi^*$ photochemistry. The photochemical pathways in clusters vary from those in isolated molecule, and yet again they are different in the various excited states.

The imidazole dimer can be considered as the simplest model for ultrafast hydrogen bond photochemistry in DNA bases. Note also at this point that after the isolated imidazole molecule absorbs photons and quenches into the ground state, the molecule disintegrates into various fragments. One can expect that within the hydrogen transfer process the excitation energy is dissipated between the donor and acceptor molecule. Imidazole units will not then have enough energy to fragment. The hydrogen transfer mechanism thus increases the photostability of the imidazole molecule in two ways: first, it allows for the ground state to be reconstructed, and second, it mediates ultrafast dissipation of excessive vibrational energy. Unfortunately, it is not possible to estimate from our experiment to what extent the hydrogen transfer mechanism is involved in the imidazole photochemistry.

IV. Conclusions

In this study, we present photodissociation of imidazole clusters of various mean sizes $\bar{n}$ of approximately $\bar{n} = 2$, 3, and 6 at wavelengths of 243 and 193 nm. The major conclusions are as follows:

(I) In resemblance to the photodissociation of a single imidazole molecule, the kinetic energy spectrum of the outgoing hydrogen atom has a bimodal character. The fast component

results from the direct dissociation on the $\pi\sigma^*$ state and the slow component from the statistical dissociation in the vibrationally hot ground state.

(II) The shape of the KED spectrum of the slow component suggests that two photons were absorbed successively before the molecule dissociates. On the other hand, the fast component corresponds to the direct adiabatic dissociation process occurring readily after the first photon absorption.

(III) With increasing cluster size, the slow component increases in intensity with respect to the fast component at 243 nm. Ab initio calculations suggest that even for larger clusters the N−H···N structural motif will always be present. It is, however, not possible at this point to decide whether the hydrogen transfer will be actively involved in the increased photostability of the imidazole clusters or whether the enhanced regeneration of the ground state is caused simply by closing the $\pi\sigma^*$ reaction channel, similarly as in the pyrrole clusters.[10]

(IV) The slow component is also dominant at the shorter wavelength of 193 nm, as has been observed previously for the molecule.[1] At this higher energy the photodissociation starts with the excitation of the $\pi\pi^*$ state as opposed to the $\pi\sigma^*$ state excited at 243 nm.

It is also worth noting that the successive two-photon hydrogen generation implicated here has been recently observed in photodissociation of acetylene clusters.[39] These processes seem to readily occur in larger systems with many degrees of freedom (i.e., clusters or large molecules), where the deposited energy can be distributed over the system, if suitable conical intersections exist between the potential hypersurfaces, which prevents the system from an immediate decay. Provided that the photon flux and the absorption cross section are large enough, a second photon can be absorbed, promoting the partly relaxed system to an excited state again, where it can dissociate.

Acknowledgment. Support by the special program "Nanotechnology for society" of the Czech Academy of Sciences via grant Nr. KAN400400651, grant Nr. KJB400400902, and grant Nr. 203/09/0422 of the Grant Agency of the Czech Republic are acknowledged. M.F. acknowledges a special J. E. Purkyně fellowship of the Czech Academy of Sciences.

References and Notes

(1) Devine, A. L.; Cronin, B.; Nix, M. G. D.; Ashfold, M. N. R. *J. Chem. Phys.* **2006**, *125*, 184302.

(2) Ashfold, M. N. R.; Cronin, B.; Devine, A. L.; Dixon, R. N.; Nix, M. G. D. *Science* **2006**, *312*, 1637.

(3) Schwell, M.; Jochims, H.-W.; Baumgärtel, H.; Leach, S. *Chem. Phys.* **2008**, *353*, 145.

(4) Jagoda-Cwiklik, B.; Slavíček, P.; Cwiklik, L.; Nolting, D.; Winter, B.; Jungwirth, P. *J. Phys. Chem. A* **2008**, *112*, 3499.

(5) Machado, F.; Davidson, E. *J. Chem. Phys.* **1992**, *97*, 1881.

(6) Serrano-Andres, L.; Fulscher, M.; Roos, B.; Merchan, M. *J. Phys. Chem.* **1996**, *100*, 6484.

(7) Su, M. *J. Phys. Chem. A* **2007**, *111*, 1567.

(8) Barbatti, M.; Lischka, H.; Salzmann, S.; Marian, C. *J. Chem. Phys.* **2009**, *130*, 034305.

(9) Sobolewski, A. L.; Domcke, W. *Phys. Chem. Chem. Phys.* **2002**, *4*, 4.

(10) Poterya, V.; Profant, V.; Fárník, M.; Slavíček, P.; Buck, U. *J. Chem. Phys.* **2007**, *127*, 064307.

(11) Rubio-Lago, L.; Zaouris, D.; Sakellariou, Y.; Sofikitis, D.; Kitsopoulos, T. N.; Wang, F.; Yang, X.; Cronin, B.; Devine, A. L.; King, G. A.; Nix, M. G. D.; Ashfold, M. N. R. *J. Chem. Phys.* **2007**, *127*, 064306.

(12) Lipciuc, M.; Wang, F.; Yang, X.; Kitsopoulos, T.; Fanourgakis, G.; Xantheas, S. *Chem. Phys. Chem.* **2008**, *9*, 1838.

(13) David, O.; Dedonder-Lardeux, C.; Jouvet, C.; Kang, H.; Martrenchard, S.; Ebata, T.; Sobolewski, A. *J. Chem. Phys.* **2004**, *120*, 10101.

(14) Kumar, A.; Kolaski, M.; Kim, K. *J. Chem. Phys.* **2008**, *128*, 034304.

(15) Frutos, L.; Markmann, A.; Sobolewski, A.; Domcke, W. *J. Phys. Chem. B* **2007**, *111*, 6110.

(16) Baumfalk, R.; Buck, U.; Frischkorn, C.; Gandhi, S. R.; Lauenstein, C. *Ber. Bunsen-Ges. Phys. Chem.* **1997**, *101*, 606.

(17) Buck, U. *J. Phys. Chem. A* **2002**, *106*, 10049.

(18) Slavíček, P.; Jungwirth, P.; Lewerenz, M.; Nahler, N. H.; Fárník, M.; Buck, U. *J. Chem. Phys.* **2004**, *120*, 4498.

(19) Fárník, M.; Nahler, N. H.; Buck, U.; Slavíček, P.; Jungwirth, P. *Chem. Phys.* **2005**, *315*, 161.

(20) Baumfalk, R.; Buck, U.; Frischkorn, C.; Nahler, N. H.; Hüwel, L. *J. Chem. Phys.* **1999**, *111*, 2595.

(21) Buck, U.; Meyer, H. *Phys. Rev. Lett.* **1984**, *52*, 109.

(22) Profant, V.; Poterya, V.; Fárník, M.; Slavíček, P.; Buck, U. *J. Phys. Chem. A* **2007**, *111*, 12477.

(23) The complete scattering experiment yielding the fragmentation probabilities of the clusters after ionization includes also measurements of the velocity distributions of the individual ionic fragments at various scattering angles (see, e.g., refs 24 and 25), which is, however, beyond the scope of the present experiment.

(24) Buck, U.; Meyer, H. *J. Chem. Phys.* **1986**, *84*, 4854.

(25) Buck, U. *J. Phys. Chem.* **1988**, *92*, 1023.

(26) Zhao, Y.; Truhlar, D. G. *Acc. Chem. Res.* **2008**, *41*, 157.

(27) Grimme, S. *J. Comput. Chem.* **2006**, *27*, 1787.

(28) Elstner, M.; Hobza, P.; Frauenheim, T.; Suhai, S.; Kaxiras, E. *J. Chem. Phys.* **2001**, *114*, 5149.

(29) Laskin, J.; Lifshitz, C. *J. Mass Spectrom.* **2001**, *36*, 459.

(30) Pinaré, J. C.; Baguenard, B.; Bordas, C.; Broyer, M. *Phys. Rev. Lett.* **1998**, *81*, 2225.

(31) Lépine, F.; Bordas, C. *Phys. Rev. A* **2004**, *69*, 053201.

(32) Frisch, M. J.; et. al. Gaussian 03, revision C.02; Gaussian, Inc.: Pittsburgh, PA, 2003.

(33) Neese, F. *ORCA—An ab initio, DFT and semiempirical SCF-MO package*, version 2.6; Lehrstuhl für Theoretische Chemie: Wegelerstrasse 12, D-53115 Bonn, Germany, 2007; see http://www.thch.uni-bonn.de/tc/orca/.

(34) Bylaska, E. J.; et al. NWChem, A Computational Chemistry Package for Parallel Computers, version 5.1; Pacific Northwest National Laboratory, Richland, WA, 2007.

(35) Choi, M.; Miller, R. *J. Phys. Chem. A* **2006**, *110*, 9344.

(36) As mentioned in the Methods the LAB angular distribution can provide an approximate information about the neutral cluster sizes. Further information could be obtained from fragmentation probabilities measurement. This would require a complete scattering experiment with velocity distribution measurements for various fragments, which was, however, beyond the scope of the present experiment. Therefore, a complementary confirmation of the mean cluster sizes was obtained by comparison to the pyrrole clusters, which exhibited mass spectra with very similar fragment size distributions, and for which the complete scattering experiment was performed.[22]

(37) It ought to be noted that we probe our molecular beam approximately 1 m downstream from the nozzle in our experiment, as opposed to most photodissociation experiments, where the expansions are probed centimeters downstream from the nozzle. Since our beam passes through the skimmer and several restraining orifices, the core containing the larger heavier species is mostly probed by the laser. Therefore, we usually obtain much better signals for cluster species than for bare molecules.

(38) It is worth noting that the fragments with the lower kinetic energy are detected with a higher probability than the faster ones and this detection probability is taken into account in the TOF → KED conversion, enhancing the fast fragment peak in the KED with respect to the slow fragment maximum.

(39) Fárník, M.; Poterya, V.; Votava, O.; Ončák, M.; Slavíček, P.; Dauster, I.; Buck, U. *J. Phys. Chem. A* **2009**, *113*, 7322.

JP904145Q